SIViP
DOI 10.1007/s11760-013-0487-5

ORIGINAL PAPER

A new approach for high density saturated impulse noise removal using decision-based coupled window median filter

Vivek Singh Bhadouria · Dibyendu Ghoshal · Abul Hasan Siddiqi

Received: 22 March 2012 / Revised: 25 November 2012 / Accepted: 20 March 2013

Abstract A new decision-based algorithm has been proposed for the restoration of digital images which are highly contaminated by the saturated impulse noise (i.e., salt-and-pepper noise). The proposed denoising algorithm performs filtering operation only to the corrupted pixels in the image, keeping uncorrupted pixels intact. The present study has used a coupled window scheme for the removal of high density noise. It has used sliding window of increasing dimension, centered at any pixel and replaced the noisy pixels consecutively by the median value of the window. However, if the entire pixels in the window are noisy, then the dimension of sliding window is increased in order to obtain the noise-free pixels for median calculation. Consequently, this algorithm has been found to be able to remove the high density salt-and-pepper noise and also preserved the fine details of the four images, Lena, Elaine, Rhythm, and Sunny, used as test images in this study (The latter two real-life images have been acquired using Sony: Steady Shot DSC- S3000). Experimentally, it has been found that the proposed algorithm yields better peak signal-to-noise ratio, image enhancement factor, structural similarity index measure and image quality index, compared with the other state-of-art median-based filters viz. standard median filter, adaptive median filter, progressive switched median filter, modified decision-based algorithm and modified decision-based unsymmetric trimmed median filter.

Keywords Coupled window · Decision-based noise removal · Median filter · Salt and pepper noise

V. S. Bhadouria · D. Ghoshal (✉)
Department of Electronics and Communication Engineering,
National Institute of Technology, Agartala 799055,
Tripura (West), India
e-mail: tukumw@gmail.com

V. S. Bhadouria
e-mail: vivek@hotmail.de

A. H. Siddiqi
S-10, Administrative Block, Gautam Buddha University,
Gautam Buddha Nagar, Greater Noida 201308,
Uttar Pradesh, India

1 Introduction

Salt-and-pepper noise occurs randomly as impulse in any image and is caused due to bit error during transmission of the image signal or introduced during the signal acquisition stage [1]. The main property of the salt-and-pepper noise is that they have only two intensity values, i.e., 0 and 255 in any 8-bit gray-scale image [2,3]. Thus, intrusion of noise degrades the image quality and causes the loss of fine image details.

It is a standard signal processing requirement to utilize filters of appropriate dimension to remove the noise by preserving the image boundary and to keep the level of blurring of the image details to a minimum [4]. When the noises are non-additive, linear filters fail to carry out the task, and nonlinear filtering techniques are most often resorted to implement the noise cleaning operation. Several nonlinear filters have been proposed for the restoration of images, corrupted by salt-and-pepper noise [5–7]. Out of them, a class of widely used nonlinear digital filter is median filter, for their inherent capability of removing the salt-and-pepper noise and other impulse noises by preserving the image boundaries [8]. For a noisy image $I(i, j)$, corrupted by impulse noise, median filtering operation can be mathematically written as

$$K(i, j) = \text{median}\{I(i, j), (i, j) \in W\} \quad (1)$$

where $K(i, j)$ is the restored image and W represents a spatial window around a pixel, centered on any location (i, j).

Published online: 04 June 2013

It has been reported that SMF is effective only for low noise density and causes blurring for large window sizes. If the window dimension is decreased to control the level of blurring, then the small window dimension leads to ineffective noise suppression [9,10].

Generally, most of the median filters operate uniformly across the image and thereby tend to modify both noisy and noise-free pixels [11]. Ideally, the filtering action should be carried out only to the noisy pixels and keeping remaining pixels of the contaminated image unchanged. Therefore, a noise detection process to distinguish between the noisy pixels and noise-free pixels, before applying nonlinear filtering operation, is essential [12–14]. To fulfill the objective, various types of median filters viz. adaptive median filter (AMF), decision-based or switching median filters have been attempted. In these filters, possible noisy pixels are identified and replaced using the median value or variants, and the uncorrupted pixels are kept intact. When the numbers of noise affected image pixels are high, i.e., noise density is high, a large size spatial filter (variants of median filter) would be needed and this would offer better noise removal but at the same time blurs the image features and the boundaries. As an example, AMF performs well at low noise densities but in case of high noise density, window dimension has to be increased which may lead to blurring of image details.

The main problem regarding the decision-based or switching median filter is that they cannot be used due to difficulty in defining a robust decisive measure arising out of proper thresholding during decision making operation [14]. Furthermore, the noisy pixels are replaced by some median value in their vicinity without taking into account local property like probable presence of edges, contours, etc. Thus, when the noise density is high, image details and edges are not completely restored. A two-phase algorithm to surmount this problem was proposed by Chan and Nikolava [15]. In the first phase, an AMF was used for the classification of noisy and noise-free pixels. This was followed, in the second phase, by application of a specialized regularization method to the noisy pixel and the method was found to be successful in preserving the edge and suppression of noise, but this algorithm had some problem due to larger processing time and larger window dimension [15,16].

To overcome the above drawbacks, Sreenivasan and Ebenezer proposed decision-based algorithm (DBA) [16]. In DBA, denoising is performed using fixed window dimension of 3×3. If the pixel's intensity is 0 or 255, it is processed for filtering, otherwise it is left unaltered. This algorithm poses a serious problem of ineffective filtering at high noise density. At a high noise density, median of the window will be again either 0 or 255 (in the case, if a window contains 0 and/or 255 pixel values only) which is again a noisy pixel value. In such situation, DBA considers neighboring pixels for replacement. However, repeated placement of neighboring pixels produces streaking effect [17]. This problem was solved by MDBA algorithm, in which if the selected window contained all 0's and/or 255's, then the trimmed value could not be calculated. Therefore, this algorithm does not work well at a higher noise density [18]. The ambiguity in handling noisy pixels was reconsidered in MDBUTMF algorithm [19]. This algorithm too considers fixed window dimension of 3×3 for the denoising purpose. This algorithm performs fairly well at lower noise density. However, it poses serious problems of ineffective noise removal at higher noise density. At a higher noise density, MDBUTMF calculates the mean of the processing window (if all the elements in the window are 0 and/or 255). However, at a higher noise density, the probability of the event that the entire pixels (in the local window) are noisy is high. Therefore, this replacement produces dark patch-like surface in the restored image. Moreover, mean-based replacement is intuitive as there is no established mathematical relation between the mean of the noisy pixel (occurrence of noise, in any image is a statistically independent process) and original, central pixel value.

In the proposed decision-based coupled window median filter (DBCWMF) algorithm, the above problem has been overcome by considering windows of increasing dimension. The basic concept of considering the coupled window of increasing dimension is to increase the probability of finding the noise-free pixels.

In case of small window dimension (i.e., 3×3), the probability that entire pixels are noisy is high. However, similar probability under same noise density reduces for larger window dimension (say, 5×5) [13]. The proposed algorithm initializes by finding noise-free pixels in 3×3 window. If all the pixels in the 3×3 window are noisy, then the dimension of the window is increased in order to find noise-free pixels. As a result, coupled windows operate in a cooperative manner toward the denoising of the image. In the first stage, DBCWMF algorithm tries to classify a pixel as either noise-corrupted or noise-free. The detailed process of verification regarding the presence of noise has been depicted in the flow chart (please refer to Fig. 1), along with the elaborate explanation in Sect. 3. If the pixel is found to be noisy, then filtering operation is performed on it. In the second phase, appropriate filtering action is taken depending upon the various cases. This decision-based filtering reduces the blurring of the image details, caused due to filtering action on noise-free as well as corrupted pixels. No study based on the decision-based sequential operation of the coupled window in spatial domain for the removal of impulse noise has been found in the published or online literature.

The organization of the paper is as follows. A short detail of noise model is given in Sect. 2. Section 3 focuses on the

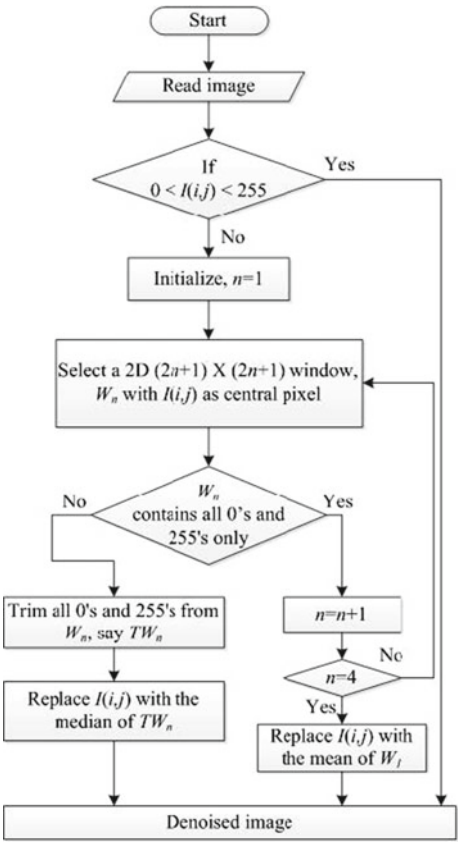

Fig. 1 Flowchart of DBCWMF algorithm.

formulation of the proposed DBCWMF algorithm. Section 4 reports a number of experimental results to demonstrate the performance of the new algorithm. Finally, conclusions are drawn in Sect. 5.

2 Noise model

In the present work, following salt-and-pepper noise model has been considered to develop a spatial filter for the removal of high density salt-and-pepper noise from the corrupted image [2,20].

In this model, the probability of occurrence of "salt" (pixel intensity of 255) and "pepper" (pixel intensity of 0) noise in any image is same. Let P_1 and P_2 be the occurrence probability for "salt" and "pepper" noise, respectively, in any gray-scale image $I(i, j)$. Mathematically, it can be written as

$$X(i,j) = \begin{cases} I(i,j) & \text{with probability } (1-\text{npr}) \\ P_1 & \text{with probability } \frac{\text{npr}}{2} \\ P_2 & \text{with probability } \frac{\text{npr}}{2} \end{cases} \quad (2)$$

where $X(i, j)$ is the resultant image and npr is the total probability of occurrence of noise.

Considering the above model, it can be concluded to use the pixel level decision algorithm in order to efficiently handle the above-mentioned noise model as the probability occurrence of salt-and-pepper noise varies from pixel to pixel [21].

3 Proposed DBCWMF algorithm

Trimming-based filters reject the noisy pixels from the 3×3 window, depending upon a predefined threshold. Alpha Trimming Mean Filtering (ATMF) is an example of a symmetrical trimming filter, which symmetrically trims the pixel from both the ends [11]. However, such symmetrical operation also leads to the rejection of some noise-free pixels which is undesirable in any filtering operation. To overcome such problem, unsymmetrical trimming filters were proposed. In an unsymmetrical trimmed median filter, pixel values (in a processing window of dimension 3×3) are arranged in ascending or descending order of their intensity values. This step is followed by trimming all the 0's and 255's (i.e., noisy pixel; 0- pepper noise; 255-salt noise) from the window and then the median value of the remaining pixel is calculated. This median value is used to replace the central noisy pixel of the processing window [18]. However this approach is ineffective at higher noise density, as discussed in Sect. 1. In the proposed algorithm, the above problem has been overcome by considering windows of increasing dimension for each noisy pixel. The proposed steps of the DBCWMF algorithm for any gray-scale image are as follows (please refer to Fig. 1):

Step 1 The first step in the proposed DBCWF algorithm is to define a local window in which the algorithm operates in order to replace the noisy pixels with the noise-free pixels.

WINDOW SELECTION: Select a 2-D window of $(2n+1) \times (2n+1)$ dimension, say W_n. Let the central pixel under consideration be $I(i, j)$ for W_n sliding window. (Initialize the algorithm by selecting $n = 1$.)

Step 2 The second step in the proposed algorithm is to find out the noisy pixel. For this purpose, proposed algorithm uses a simple rule, mentioned in the Eq. (3). Salt-and-pepper noise-corrupted pixels can take either 0 or 255 intensity values only. Therefore, such noisy pixels can be easily identified by comparing the pixel value with 0 and 255.

NOISY PIXEL DETECTION: If $I(i, j)$=0 or 255, then it is a noise-corrupted pixel and should be processed [19]. This detection process can be written as

$$K(i,j) = \begin{cases} \text{noisy pixel} & \text{if } I(i,j) = 0 \text{ or } 255 \\ \text{noise-free pixel} & \text{if } 0 < I(i,j) < 255 \end{cases} \quad (3)$$

If $0 < I(i, j) < 255$, then $I(i, j)$ is an uncorrupted pixel and it should be left intact.

Step 3 If a pixel is found to be noisy, then the DBCWMF algorithm uses the neighbor pixels of the local window (discussed in step 1) around $I(i, j)$ to operate filtering on the central pixel. DBCWMF performs filtering action by removing all the 0's and 255's from the window, followed by median calculation of the remaining pixels. At a higher noise density, the local window may contain all the noisy pixels. In such cases, the dimension of the local window is increased in order to find the noise-free pixels for median calculation.

FILTERING OPERATION: If $I(i, j)$ =0 or 255, then trim all the 0's and 255's from the W_n window. Let the new processed, trimmed window be TW_n. After trimming, the noisy pixels following cases are possible

Case 1 If the number of elements in TW_n are non-zero, then $I(i, j)$ can be replaced as

$$K(i, j) = \{\text{median}(TW_n)\} \tag{4}$$

where $K(i, j)$ is the restored value.

Case 2 If the number of elements in TW_n is zero, then update the value of n as ($n < 5$):

$$n = n + 1 \tag{5}$$

And go to step 1.

Step 4 The size of the local window is increased upto $n < 5$ in order to search the noise-free pixels. Increasing the local window dimension beyond $n \geq 5$ will increase the computational complexity of the algorithm. Additionally, the calculated median (obtained by setting $n \geq 5$) will be less correlated with the $I(i, j)$'s neighborhood. If all the pixels are found to be noisy for $n = 4$, then the algorithm replaces the noisy pixel with the mean of W_1.

If the number of elements in TW_4 is zero, then replace $I(i, j)$ as

$$K(i, j) = \text{mean}(W_1) \tag{6}$$

Step 5 Repeat steps 1–4 in *for* loop until all the pixels of the image are processed.

The flow chart representation of proposed algorithm is shown in Fig. 1.

For a multichannel image (like RGB color space), the above-mentioned algorithm needs to be separately operated on each color channel. After the denoising operation, separate channels can be aggregated to get a denoised color image.

4 Results and discussion

The performance of DBCWMF proposed algorithm has been evaluated and compared with some of the state-of-art median-based filters. In the present study, standard color image (Lena, dimension: 512 × 512 × 3) and gray-scale image (Elaine, dimension: 512 × 512) along with two natural images, captured using Sony: Steady Shot DSC-S3000 (Rhythm, dimension: 256 × 256 and Sunny, dimension: 400 × 369 × 3) have been used, with varying noise density, ranging from 10 % to 90 %. Two natural images have been considered in order to study the performance of algorithms in real-life environment

Fig. 2 Simulation results of different algorithms for Lena image at 30 % noise density. **a** Original image; **b** Noise-corrupted image; **c** Output of SMF; **d** Output of AMF; **e** Output of PSMF; **f** Output of MDBA; **g** Output of MDBUTMF; **h** Output of DBCWMF

Fig. 3 Simulation results of different algorithms for Lena image at 70 % noise density. **a** Noise-corrupted image; **b** Output of SMF; **c** Output of AMF; **d** Output of PSMF; **e** Output of MDBA; **f** Output of MDBUTMF; **g** Output of DBCWMF

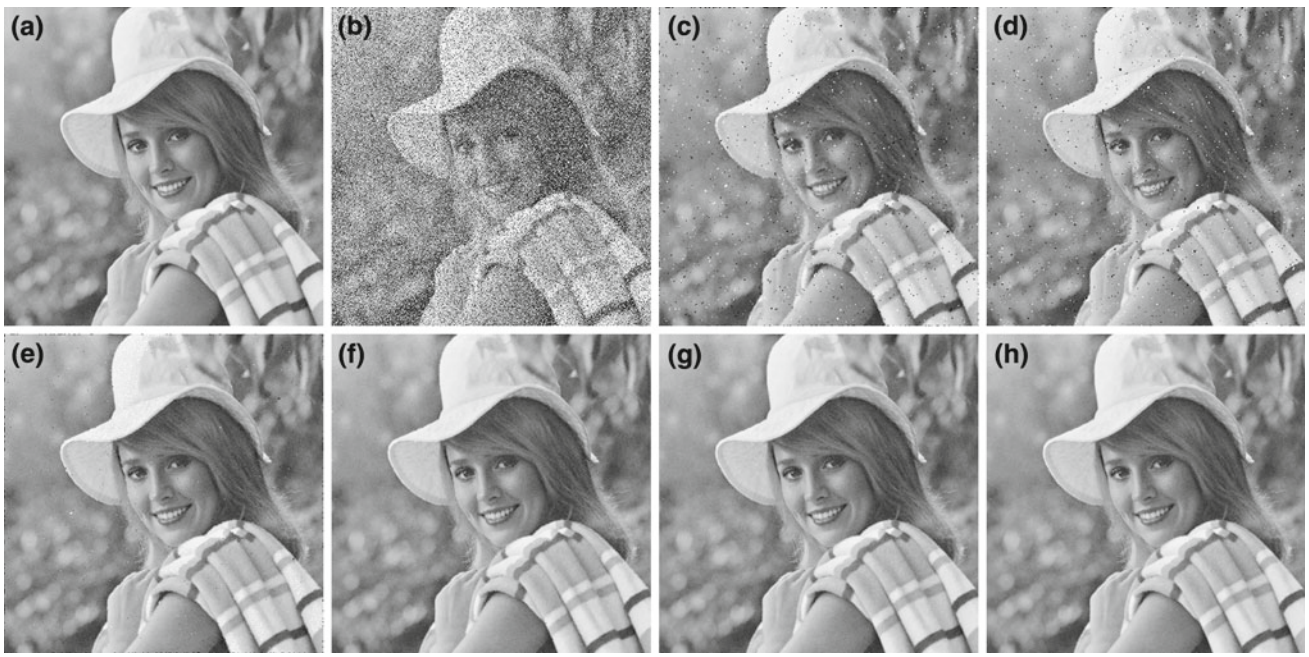

Fig. 4 Simulation results of different algorithms for Elaine image at 30 % noise density. **a** Original image; **b** Noise corrupted image; **c** Output of SMF; **d** Output of AMF; **e** Output of PSMF; **f** Output of MDBA; **g** Output of MDBUTMF; **h** Output of DBCWMF

(e.g., inside the house or hall) where illumination fluctuation may occur.

Denoising performance of proposed algorithm has been evaluated on the basis of quantitative performance criteria of peak signal-to-noise ratio (PSNR), image enhancement factor (IEF) [16,19], structural similarity index measure (SSIM) [22], and image quality index (IQI) [23], as given in Eqs. (7), (8), (9) and (12), respectively.

$$\mathrm{PSNR} = 20\log_{10}\left(\frac{255}{\frac{1}{AB}\sum_{i=1}^{A}\sum_{j=1}^{B}\{I\,(i,\,j) - K\,(i,\,j)\}^2}\right) \tag{7}$$

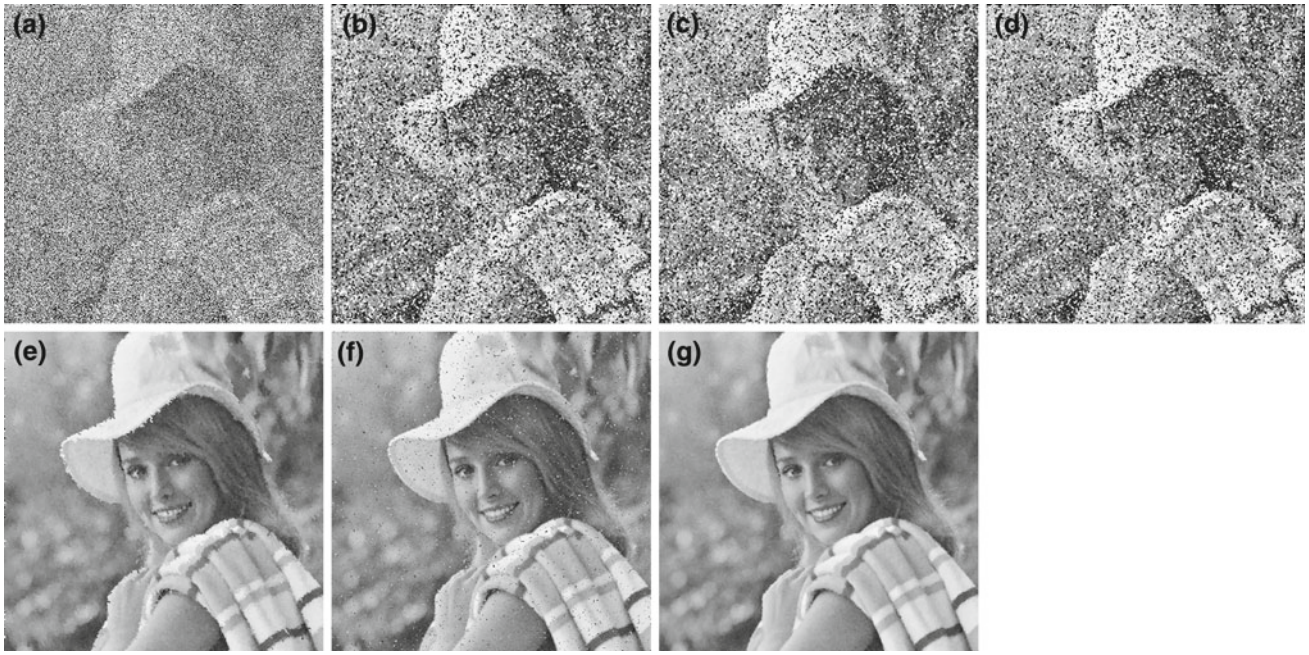

Fig. 5 Simulation results of different algorithms for Elaine image at 70 % noise density. **a** Noise-corrupted image; **b** Output of SMF; **c** Output of AMF; **d** Output of PSMF; **e** Output of MDBA; **f** Output of MDBUTMF; **g** Output of DBCWMF

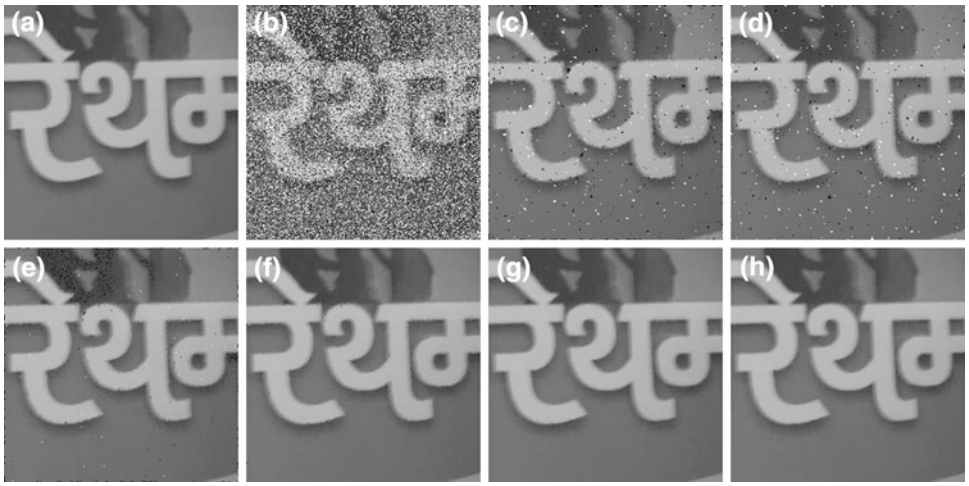

Fig. 6 Simulation results of different algorithms for Rhythm image at 30 % noise density. **a** Original image; **b** Noise corrupted image; **c** Output of SMF; **d** Output of AMF; **e** Output of PSMF; **f** Output of MDBA; **g** Output of MDBUTMF; **h** Output of DBCWMF

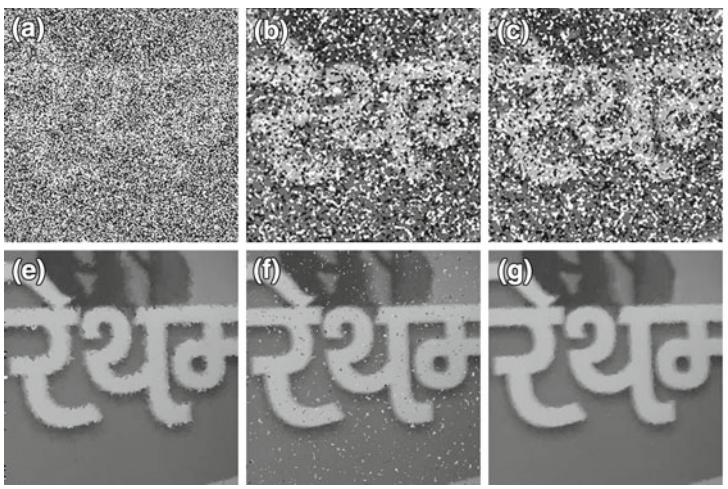

Fig. 7 Simulation results of different algorithms for Rhythm image at 70 % noise density. **a** Noise-corrupted image; **b** Output of SMF; **c** Output of AMF; **d** Output of PSMF; **e** Output of MDBA; **f** Output of MDBUTMF; **g** Output of DBCWMF

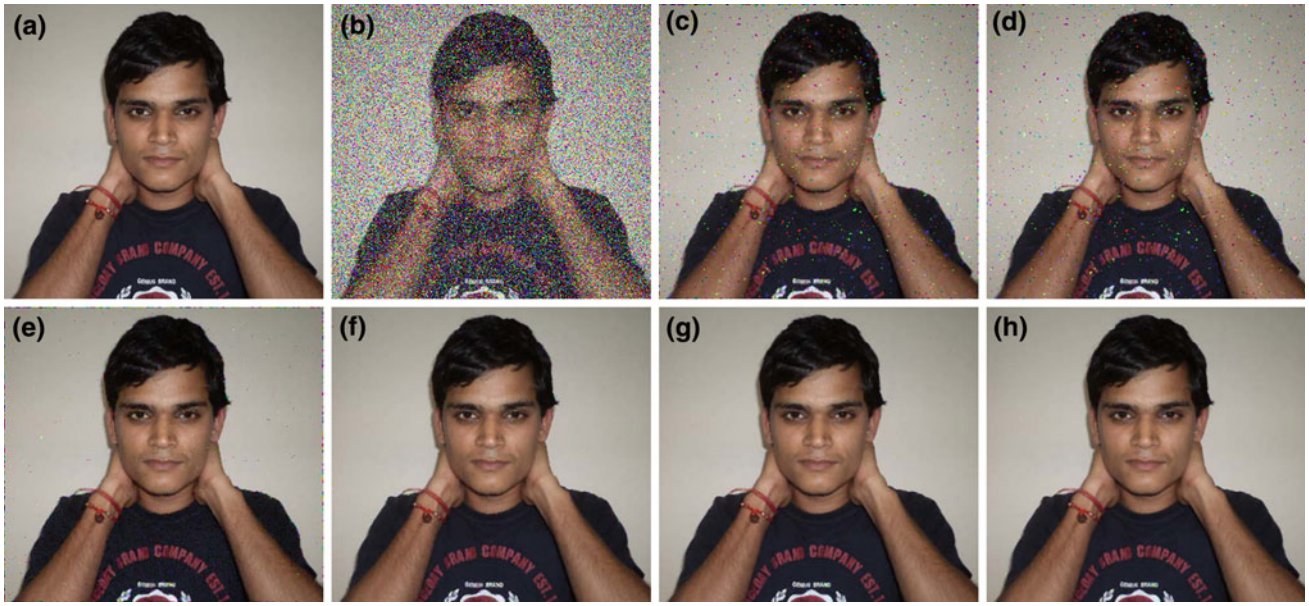

Fig. 8 Simulation results of different algorithms for Sunny image at 30 % noise density. **a** Original image; **b** Noise corrupted image; **c** Output of SMF; **d** Output of AMF; **e** Output of PSMF; **f** Output of MDBA; **g** Output of MDBUTMF; **h** Output of DBCWMF

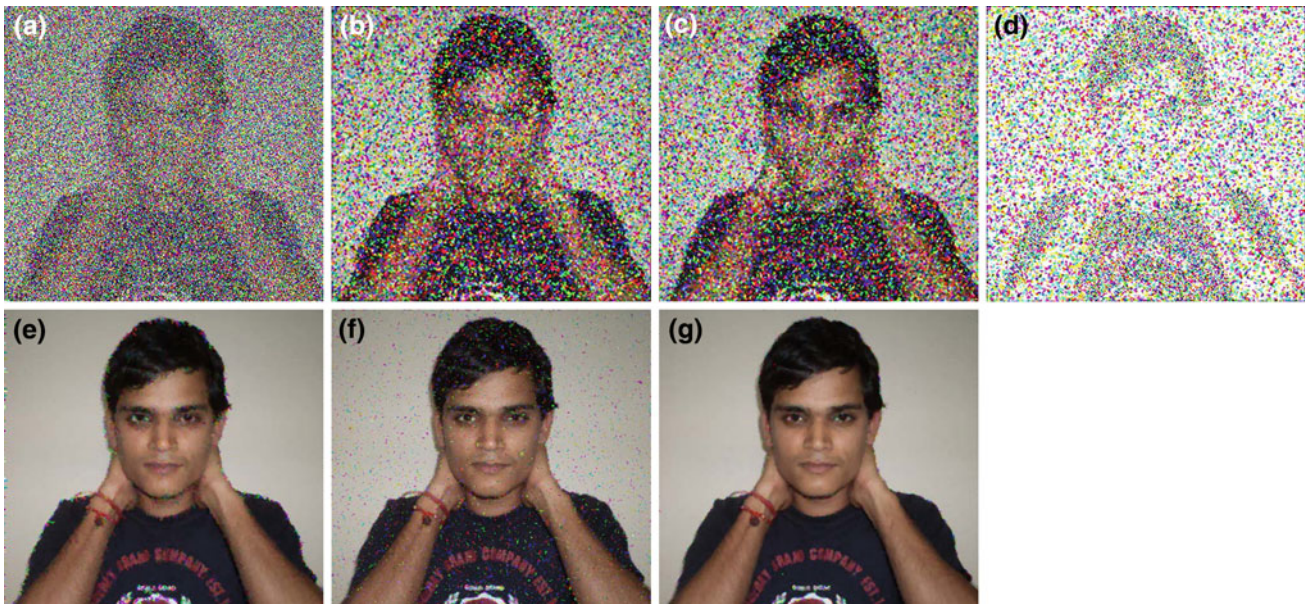

Fig. 9 Simulation results of different algorithms for Sunny image at 70 % noise density. **a** Noise-corrupted image; **b** Output of SMF; **c** Output of AMF; **d** Output of PSMF; **e** Output of MDBA; **f** Output of MDBUTMF; **g** Output of DBCWMF

$$\mathrm{SSIM}\,(I, K) = \frac{(2\mu_I\mu_K)\,(2\sigma_{IK} + C_2)}{\left(\mu_I^2 + \mu_K^2 + C_1\right)\left(\mu_I^2 + \mu_K^2 + C_2\right)} \tag{8}$$

$$\mathrm{IEF} = \frac{\sum_{i=1}^{A}\sum_{j=1}^{B}\{X\,(i,\,j) - I\,(i,\,j)\}^2}{\sum_{i=1}^{A}\sum_{j=1}^{B}\{K\,(i,\,j) - I\,(i,\,j)\}^2} \tag{9}$$

where $I\,(i,\,j)$, $X\,(i,\,j)$, and $K\,(i,\,j)$ represent original, noisy, and restored image of dimension $A \times B$, respectively. μ and σ represent mean intensity and standard deviation from the peak intensity of the images, respectively. C_1 and C_2 being the constants, σ_{IK} (i.e., standard deviation at any pixel) can be calculated as

$$\sigma_{IK} = \frac{1}{N-1}\sum_{i=1}^{N}(I_i - \mu_I)\,(K_i - \mu_K) \tag{10}$$

Better performance of the proposed DBCWMF algorithm over the other state-of-art algorithms (discussed in Sect. 1) has also been proven through the performance graph. For

Table 1 PSNR, IEF, SSIM, and IQI for various algorithms for Lena image at different noise densities

Filter type	Attribute	Noise density (%)				
		10	30	50	70	90
	PSNR (dB)	33.16	23.41	15.23	10.02	6.63
SMF	IEF	59.23	18.86	4.77	2.00	1.18
	SSIM	0.91	0.70	0.23	0.05	0.01
	IQI	0.999	0.998	0.986	0.943	0.864
	PSNR (dB)	40.34	28.72	19.78	14.39	10.91
AMF	IEF	110.99	23.28	5.01	2.05	1.19
	SSIM	0.97	0.79	0.31	0.09	0.02
	IQI	1.00	0.999	0.987	0.943	0.864
	PSNR (dB)	36.84	28.76	20.88	9.96	6.62
PSMF	IEF	138.02	64.72	17.54	1.98	1.18
	SSIM	0.98	0.90	0.57	0.05	0.01
	IQI	0.999	0.999	0.995	0.951	0.870
	PSNR (dB)	41.51	34.67	30.33	25.57	19.80
MDBA	IEF	404.65	252.41	154.37	72.07	24.56
	SSIM	0.98	0.95	0.89	0.79	0.58
	IQI	1.00	0.999	0.999	0.997	0.978
	PSNR (dB)	41.75	35.77	31.27	23.60	14.86
MDBUTMF	IEF	456.74	344.38	203.48	48.75	8.38
	SSIM	0.99	0.97	0.93	0.69	0.17
	IQI	1.00	0.999	0.999	0.998	0.959
	PSNR (dB)	41.76	35.84	32.49	29.72	25.85
DBCWMF	IEF	458.75	349.70	269.58	199.34	105.23
	SSIM	0.99	0.97	0.93	0.90	0.81
	IQI	1.00	1.00	0.999	0.999	0.993

the sake of brevity, the graphs indicating the performance of proposed algorithm have been given for Lena image only.

Generally, denoising algorithms are an integral part of low-level image processing [8,24]. Therefore, for an efficient imaging system, denoising algorithms should perform efficiently in order to facilitate ease to medium- or high-level image processing stages. In this work, an attempt has been made to study the effect of denoising algorithms on medium-level image processing. For this, edge map of restored Lena image, corrupted with 70 % noise density, for various discussed algorithms are also computed. Edge maps have also been quantitatively measured using Pratt's figure of merit (PFOM) [25,26]. With scaling factor a (in the present work, a = 1/9) and separation distance d, PFOM is defined as

$$\text{PFOM} = \frac{1}{I_N}\sum_{i=1}^{I_A}\frac{1}{1+ad^2} \tag{11}$$

where $I_N = \max\{I_I, I_A\}$, I_I and I_A are the ideal edge map and an actual edge map, respectively.

Additionally, algorithm performance has also been evaluated on a qualitative basis of image quality index (IQI) and visual perception. IQI is calculated by modeling any image distortion as a combination of three factors: loss of correlation, luminance distortion, and contrast distortion [20,23]. IQI is calculated using

$$\text{IQI} = \text{Corr}(I, K) \times \text{Lum}(I, K) \times \text{Cont}(I, K) \tag{12}$$

$$\text{Corr}(I, K) = \frac{\sigma_{IK}}{\sigma_I \sigma_K} \tag{13}$$

$$\text{Lum}(I, K) = \frac{(2\mu_I \mu_K)}{\left(\mu_I^2 + \mu_K^2\right)} \tag{14}$$

$$\text{Cont}(I, K) = \frac{(2\sigma_I \sigma_K)}{\left(\sigma_I^2 + \sigma_K^2\right)} \tag{15}$$

The allowed range of IQI is $[-1, 1]$ and the best value of 1 is achieved iff restored image is equal to the original image. Along with IQI calculation, image quality map (IQM) has also been calculated to evaluate the denoising performance of the proposed algorithm. Brighter IQM concludes that the restored image is closer to the original image. Conversely,

Table 2 PSNR, IEF, SSIM, and IQI for various algorithms for Elaine image at different noise densities

Filter type	Attribute	Noise density (%)				
		10	30	50	70	90
	PSNR (dB)	31.64	23.55	15.21	9.99	6.65
SMF	IEF	41.27	19.24	4.71	1.98	1.18
	SSIM	0.77	0.61	0.19	0.04	0.01
	IQI	0.999	0.999	0.990	0.956	0.881
	PSNR (dB)	35.22	24.06	15.38	10.03	6.67
AMF	IEF	94.17	21.81	4.90	2.00	1.18
	SSIM	0.90	0.72	0.23	0.04	0.01
	IQI	1.00	0.999	0.991	0.957	0.882
	PSNR (dB)	37.75	28.73	20.93	9.96	6.64
PSMF	IEF	168.25	63.54	17.59	1.97	1.17
	SSIM	0.96	0.86	0.54	0.04	0.01
	IQI	1.00	0.999	0.998	0.958	0.888
MDBA	PSNR (dB)	40.51	34.84	30.87	26.49	20.05
	IEF	318.10	259.28	173.72	88.75	25.84
	SSIM	0.97	0.91	0.83	0.71	0.49
	IQI	1.00	0.999	0.999	0.998	0.958
MDBUTMF	PSNR (dB)	41.35	35.92	32.00	24.74	16.04
	IEF	392.26	333.10	222.15	59.21	10.25
	SSIM	0.97	0.92	0.84	0.59	0.15
	IQI	1.00	1.00	0.999	0.999	0.974
	PSNR (dB)	41.36	35.93	33.02	30.46	27.08
DBCWMF	IEF	392.81	333.78	284.67	221.38	130.25
	SSIM	0.97	0.92	0.86	0.77	0.65
	IQI	1.00	1.00	0.999	0.999	0.996

darker IQM indicates more distance between the restored and original image [20].

Figures 2, 4, 6, and 8 shows the Lena, Elaine, Rhythm, and Sunny image corrupted with 30 % noise density and Figs. 3, 5, 7 and 9 show the Lena, Elaine, Rhythm, and Sunny image corrupted with 70 % noise density, respectively. From Fig. 3b, it can be easily observed that at higher noise density, SMF blurs the fine image features along with ineffective noise removal. In Fig. 3e and f, the filtered image contains sharper image details, perceptually compared to Fig. 3b, c, and d for Lena image. However, traces of the presence of salt-and-pepper noise can be seen in efficient algorithms like MDBUTMF for higher noise density, as shown in Fig. 3f. The proposed algorithm removes the noise effectively without degrading the fine image features, as shown in Fig. 3g.

Similar results have also been observed for Elaine, Rhythm, and Sunny image. Figures 5g, 7g, and 9g show the better noise removal capability along with fine detail preservation of the proposed algorithm, compared to other well-known median filters, shown in Figs. 5b–f, 7b–f, and 9b–f. Other filters (i.e., SMF, AMF, and PSMF) reduce the noise at the cost of blurring the image details, evident from lower SSIM values listed in Tables 1, 2, 3, and 4 for Lena, Elaine, Rhythm, and Sunny, respectively.

The PSNR, IEF, SSIM, and IQI values of the proposed DBCWMF algorithm are compared against the existing state-of-art, published salt-and-pepper denoising algorithms, by varying noise density, from 10 % to 90 % and are shown in Tables 1, 2, 3, and 4 for Lena, Elaine and Rhythm and Sunny images, respectively. From the quantitative values shown in Tables 1, 2, 3, and 4, it can be observed that the denoising performance of the proposed algorithm is better than existing median-based filters.

At low noise density, proposed algorithm yields slightly better *PSNR*, compared to MDBUTMF, due to the fact that the proposed algorithm increases the window dimension for denoising, if all the pixels in the window are noisy. However, MDBUTMF follows an intuitive approach and calculates the mean of the noisy 3×3 window in such situation. Increasing window dimension proves fruitful in the case if the entire pixels in the window are noisy or if the noise density is high [13], yielding high PSNR, IEF, and SSIM values. High *PSNR* value is essential for

Table 3 PSNR, IEF, SSIM, and IQI for various algorithms for Rhythm image at different noise densities

Filter type	Attribute	Noise density (%)				
		10	30	50	70	90
	PSNR (dB)	38.03	23.97	15.29	10.24	6.74
SMF	IEF	175.13	21.25	4.76	2.07	1.19
	SSIM	0.98	0.75	0.21	0.04	0.01
	IQI	1.00	0.998	0.985	0.938	0.860
	PSNR (dB)	43.03	24.79	15.60	10.11	6.72
AMF	IEF	542.36	25.22	5.08	2.02	1.19
	SSIM	0.99	0.78	0.23	0.04	0.01
	IQI	1.00	0.998	0.982	0.944	0.857
	PSNR (dB)	38.89	29.69	15.23	10.21	6.73
PSMF	IEF	213.25	79.33	4.69	2.05	1.19
	SSIM	0.98	0.71	0.21	0.04	0.01
	IQI	1.00	0.999	0.987	0.942	0.859
	PSNR (dB)	47.78	39.33	33.92	27.67	19.82
MDBA	IEF	1,651.60	728.17	346.46	114.53	24.29
	SSIM	0.99	0.98	0.95	0.88	0.66
	IQI	1.00	1.00	0.999	0.998	0.980
	PSNR (dB)	51.58	42.70	35.83	26.17	16.40
MDBUTMF	IEF	4,015.12	1,656.81	540.01	81.48	11.06
	SSIM	0.99	0.99	0.96	0.69	0.95
	IQI	1.00	1.00	0.999	0.998	0.959
	PSNR (dB)	51.66	43.10	38.70	35.43	30.23
DBCWMF	IEF	4,082.40	1,736.5	1,047.48	686.07	267.85
	SSIM	0.99	0.99	0.97	0.95	0.89
	IQI	1.00	1.00	0.999	0.999	0.995

subsequent image processing stages. A graphical view of PSNR, IEF, SSIM, and IQI plotted against noise density for Lena image is also shown in Figs. 10, 11, 12, and 13, respectively.

From Figs. 3g, 5g, 7g, and 9g, it can be inferred that the proposed algorithm outperforms other median-based filters in reducing the noise as well as preserving the fine image features from the corrupted image (Figs. 10, 11, 12, 13, and 14).

Figure 15 shows the IQM for restored Lena image, corrupted with 70 % noise density. It can be seen that IQM for DBCWMF algorithm is brighter (shown in Fig. 15f), compared to other IQM obtained from other algorithms (Fig. 15a–e). Superior performance is further evident from the brighter IQM for Sunny image (shown in Fig. 16), obtained using DBCWMF algorithm. A large dark area of IQM can be seen for SMF (Fig. 16a), AMF (Fig. 16b), and PSMF (Fig. 16c) algorithm which proves their poor denoising performance at high noise density. However, darker region reduces to a great extent, in the case of MDBA (Fig. 16d), MDBUTMF (Fig. 16e), and DBCWMF (Fig. 16f) algorithm. The least dark area is visible in DBCWMF algorithm's IQM, suggesting that restored image is much closer to the original image.

Figure 14a shows the edge map of original Lena image, obtained from Canny's edge detector. Figure 14b–g shows the edge map obtained from SMF, AMF, PSMF, MDBA, MDBUTMF, and DBCWMF algorithm, respectively, for restored Lena image, corrupted with 70 % noise density. Ineffective noise filtering of SMF, AMF, PSMF, and MDBUTMF algorithm can be easily seen in the Fig. 14b, c, d, and f. SMF, AMF, and PSMF algorithms are ineffective in preserving image details. Patch formation in case of MDBUTMF algorithm (as discussed in Sect. 1) is also evident in Fig 14f. These patchy surfaces make it difficult for the edge detection process. Therefore, these algorithms are not suitable for efficient imaging systems because their inefficiency may lead to wrong results in higher-level image processing operations (e.g., pattern recognition). MDBA performs quite well in preserving image details but at the same time distorts the fine details, as shown in Fig 14e. Distorted edges are not suitable for any image processing applications. Edge map obtained from DBCWMF algorithm shown in Fig. 14g preserves the fine image details and geometry, suggesting the practicabil-

Table 4 PSNR, IEF, SSIM, and IQI for various algorithms for Sunny image at different noise densities

Filter type	Attribute	Noise density (%)				
		10	30	50	70	90
	PSNR (dB)	36.74	27.32	19.54	14.00	10.36
SMF	IEF	48.96	17.78	5.12	2.09	1.20
	SSIM	0.97	0.76	0.26	0.07	0.02
	IQI	0.996	0.992	0.965	0.876	0.764
	PSNR (dB)	42.22	28.86	19.83	14.27	10.45
AMF	IEF	175.14	25.16	5.49	2.21	1.22
	SSIM	0.99	0.79	0.26	0.07	0.02
	IQI	0.997	0.993	0.955	0.875	0.762
	PSNR (dB)	23.70	22.85	20.72	13.67	10.29
PSMF	IEF	2.45	6.32	6.78	1.93	1.18
	SSIM	0.93	0.86	0.59	0.07	0.02
	IQI	0.990	0.978	0.946	0.890	0.764
	PSNR (dB)	24.05	23.96	23.77	23.14	20.67
MDBA	IEF	2.7	8.14	16.63	17.13	12.96
	SSIM	0.95	0.94	0.93	0.89	0.75
	IQI	0.999	0.986	0.979	0.972	0.950
	PSNR (dB)	44.47	37.89	32.76	2.63	14.58
MDBUTMF	IEF	865.82	573.28	292.49	50.20	7.99
	SSIM	0.99	0.99	0.96	0.70	0.21
	IQI	0.999	0.998	0.996	0.982	0.869
	PSNR (dB)	44.48	37.87	34.46	31.63	27.28
	IEF	867.51	570.26	432.54	316.17	148.95
DBCWMF	SSIM	0.99	0.99	0.98	0.93	0.88
	IQI	0.999	0.997	0.991	0.991	0.973

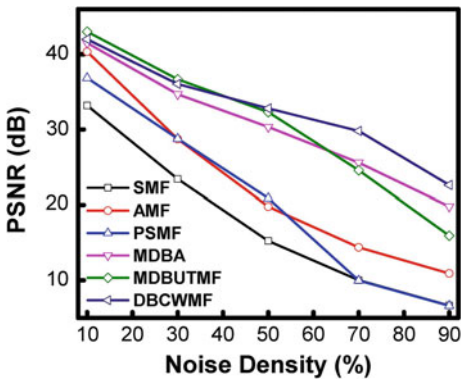

Fig. 10 Comparison graph of PSNR values at different noise densities (varying from 10 % to 90 %) for Lena image

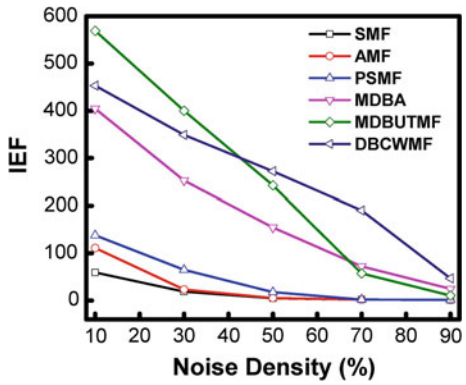

Fig. 11 Comparison graph of IEF values at different noise densities (varying from 10 % to 90 %) for Lena image

ity of the proposed algorithm. Edge preserving nature of proposed algorithm is also evident from high SSIM values for Lena, Elaine, Rhythm, and Sunny image, shown in Tables 1, 2, 3, and 4, respectively.

The edge map calculation is performed on the restored Lena image, corrupted with 70 % salt-and-pepper noise density. Table 5 lists the PFOM values for various edge maps, obtained for various discussed algorithms. Quantitative performance measure of PFOM also suggests the closeness of edge map obtained from DBCWMF algorithm and original edge map, obtained using Canny's edge detector. Higher PFOM value suggests that DBCWMF algorithm reduces the noise, along with preserving image features. Therefore, the proposed algorithm can be efficiently used in a

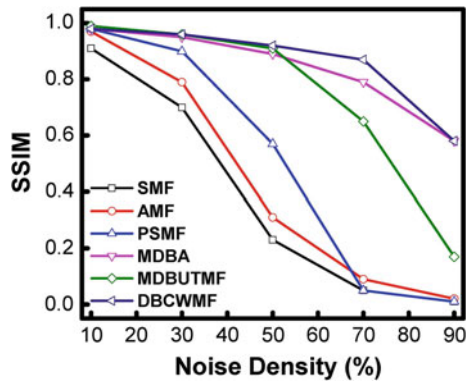

Fig. 12 Comparison graph of SSIM values at different noise densities (varying from 10 % to 90 %) for Lena image

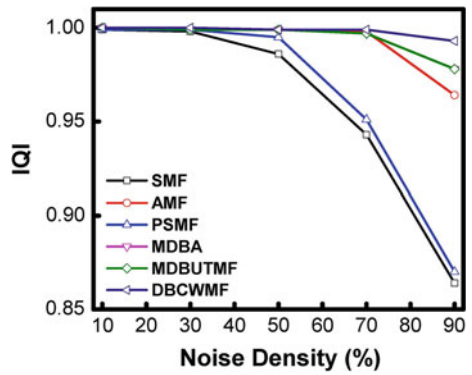

Fig. 13 Comparison graph of IQI values at different noise densities (varying from 10 % to 90 %) for Lena image

practical, efficient imaging system. Even in case of high noise density, proposed algorithm will perform well, without degrading the image quality, providing a clean image as input to the medium- or high-level image processing stages.

5 Conclusion

In this paper, an efficient decision-based, coupled window-based median filtering algorithm for the restoration of images, corrupted with high density salt-and-pepper noise, has been proposed. DWCWMF algorithm operates in two phases; first phase is a noisy pixel detection stage and the second phase is a filtering stage. Decision-based approach allows to process filtering action on noisy pixels only, reducing undue distortion and loss of image details caused due to filtering action on noise-free pixels.

DBCWMF algorithm provides slightly better results at a low noise density due to increasing window dimension consideration in the algorithm, if the entire pixels in the window are noisy. Increasing window dimension approach also proves to be advantageous in performing denoising at high noise density because for a given noise density, probability of finding a noise-free pixel is high in large window (i.e., 5×5 and above dimensions), as compared to the small window (3×3). Standard test images (Lena and Elaine) along with two natural real-life images (Rhythm and Sunny) have been used to evaluate the performance of various

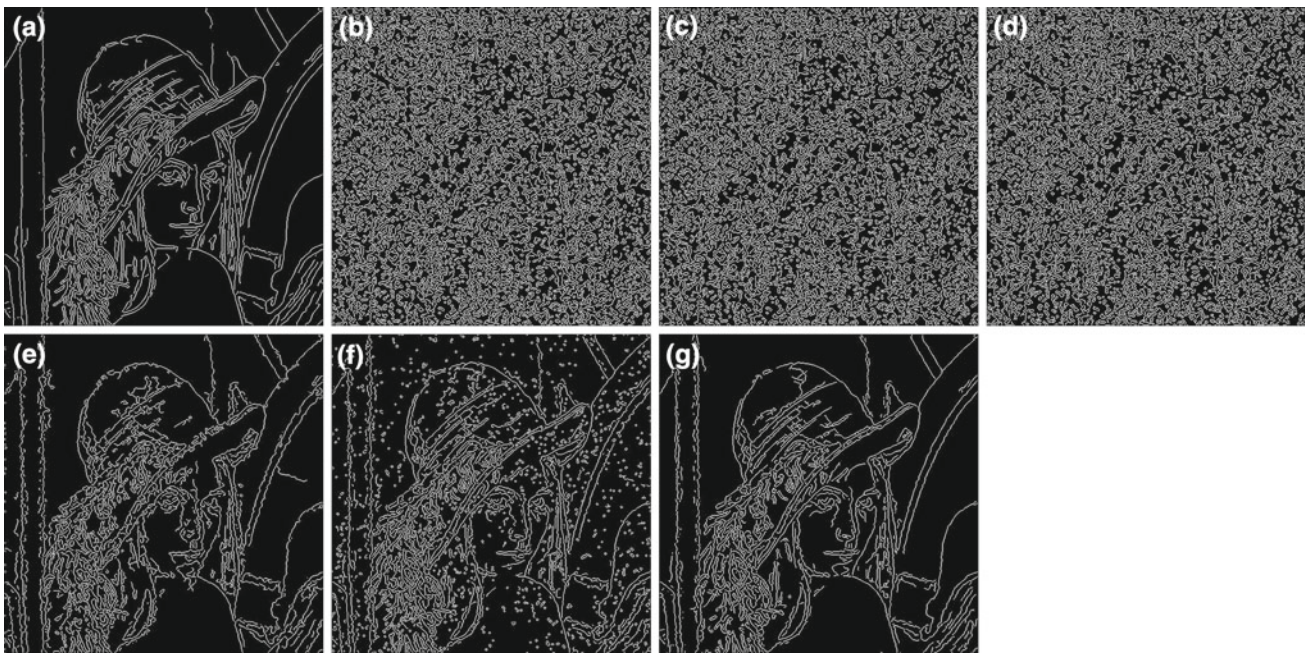

Fig. 14 **a** Edge map of original Lena image; Edge map of the restored Lena image corrupted with 70 % noise density, restored using **b** SMF; **c** AMF; **d** PSMF; **e** MDBA; **f** MDBUTMF; (g) DBCWMF

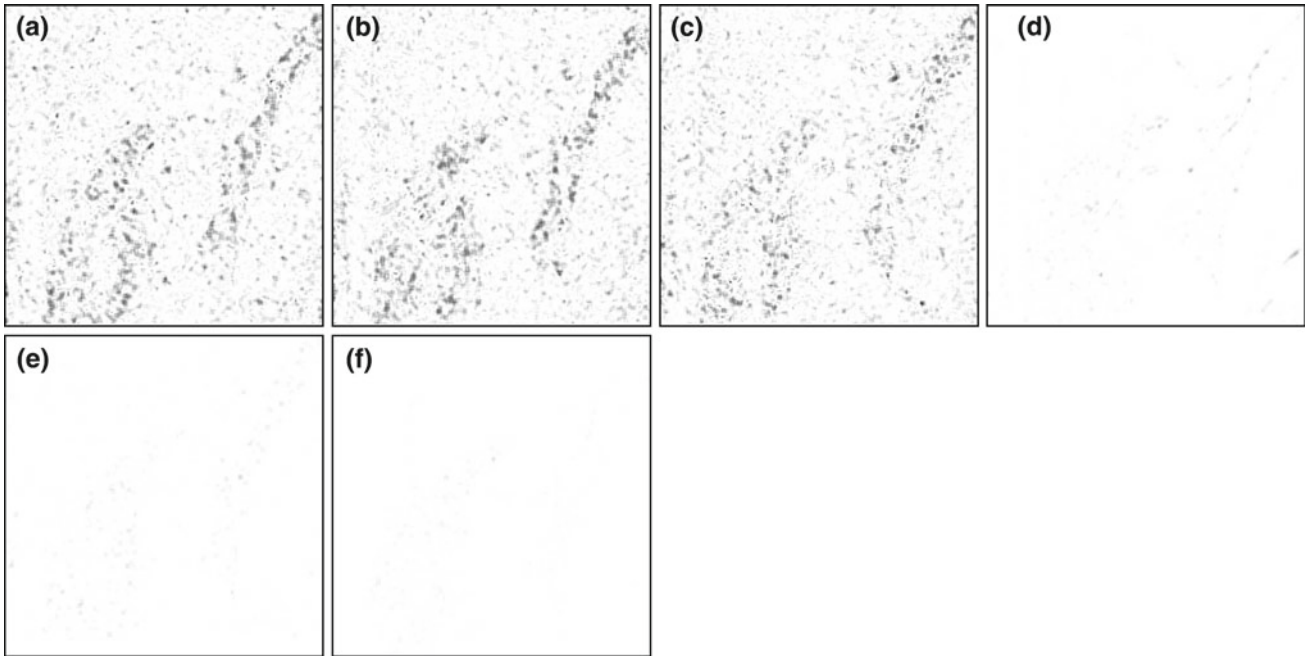

Fig. 15 Simulation results of image quality map for restored Lena image, corrupted with 70 % noise density. **a** SMF; **b** AMF; **c** PSMF; **d** MDBA; **e** MDBUTMF; **f** DBCWMF

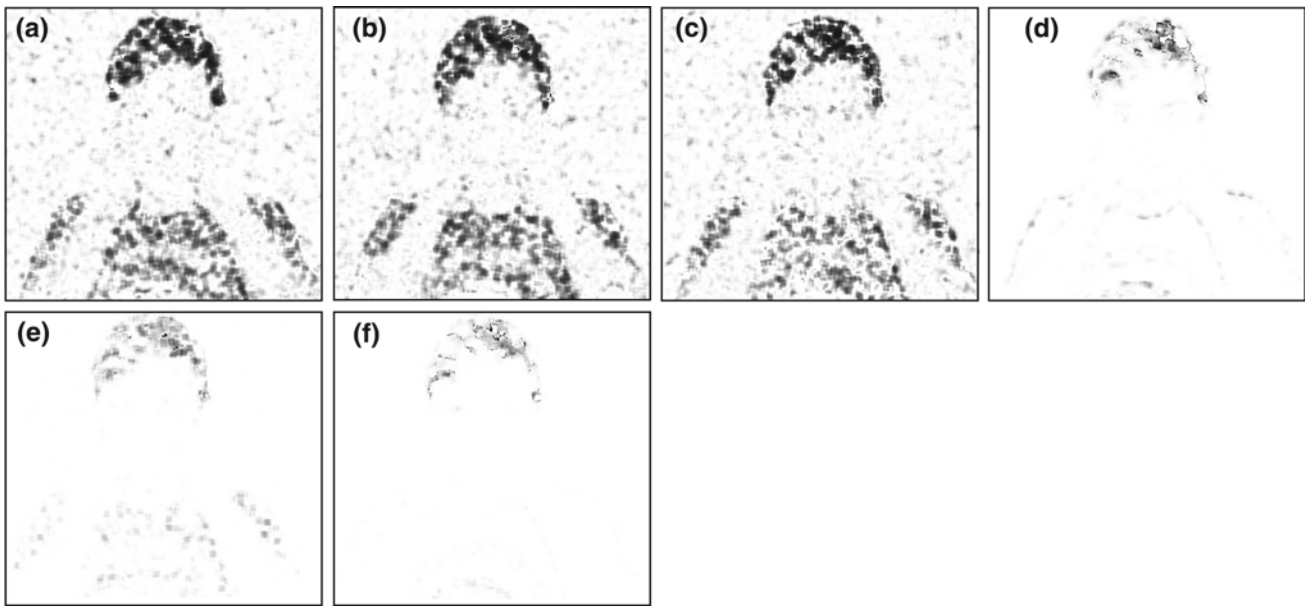

Fig. 16 Simulation results of image quality map for restored Sunny image, corrupted with 70% noise density. **a** SMF; **b** AMF; **c** PSMF; **d** MDBA; **e** MDBUTMF; **f** DBCWMF

algorithms. Experimentally, it has been found that the proposed algorithm yields better results in terms of high PSNR, IEF, SSIM, and IQI values, as compared to other state-of-art filters.

In the present work, the effect of the proposed algorithm on subsequent image processing stages has also been studied. Restored Lena image, corrupted with 70 % noise density, was used in this study. Canny's edge detector was used to obtain an edge map from restored images, obtained from SMF, AMF, PSMF, MDBA, MDBUTMF, and DBCWMF algorithm. Higher value of Pratt's figure of merit indicates that edges are preserved even after DBCWM filtering operation. This suggests the suitability of the proposed algorithm as DBCWMF denoises the image without

Table 5 Pratt's figure of merit for restored various images, corrupted with 70 % noise density for various algorithms

Filter type	Image			
	Lena	Elaine	Rhythm	Sunny
SMF	0.2985	0.2946	0.1865	0.2321
AMF	0.2997	0.2964	0.1891	0.2340
PSMF	0.2984	0.2931	0.1880	0.2329
MDBA	0.8559	0.6589	0.7870	0.8293
MDBUTMF	0.6931	0.5661	0.5721	0.5789
DBCWMF	0.9355	0.7598	0.9185	0.9495

degrading the image quality, providing a clean noise-free image as input to medium- or high-level image processing stages.

Acknowledgments The authors would like to gratefully acknowledge the kind inspiration from Prof. (Dr.) P. K. Bose, Director, National Institute of Technology, Agartala, India, to carry out the research work. DG dedicates the research work to loving and everlasting memory of Late. Ms. Sumita Ghoshal, the only sister of DG, who herself was a gem of scholar, symbol of wisdom and wit, beauty and simplicity.

References

1. Umbaugh, S.E.: Computer Vision and Image Processing. Prentice-Hall, Eaglewood Cliffs (1998)
2. chulte, S., Nachtegael, M., Witte, V.D., Weken, D.V., Kerre, E.E.: A fuzzy impulse noise detection and reduction method. IEEE Trans. Image Process. **15**(5), 1153–1162 (2006)
3. Schulte, S., Witte, V.D., Nachtegael, M., Weken, D.V., Kerre, E.E.: Fuzzy two-step filter for impulse noise reduction from color images. IEEE Trans. Image Process. **15**(11), 3568–3579 (2006)
4. Lee, J.-S., Jurkevich, I., Dewaele, P., Wambacq, P., Oosterlinck, A.: Speckle filtering of synthetic aperture radar images: a review. Remote Sens. Rev. **8**, 313–340 (1994)
5. Hwang, H., Haddad, R.A.: Adaptive median filters: new algorithms and results. IEEE Trans. Image Process. **4**(4), 499–502 (1995)
6. Hamza, A.B., Luque, P., Martinez, J., Roman, R.: Removing noise and preserving details with relaxed median filters. J. Math. Image Vis. **11**(2), 161–177 (1999)
7. Huang, T.S., Yang, G.J., Tang, G.Y.: Fast two-dimensional median filtering algorithm. IEEE Trans. ASSP **1**(1), 13–18 (1979)
8. Gonzalez, R.C., Woods, R.E.: Digital Image Processing. Pearson Education, Singapore (2002)
9. Pitas, I.: Digital Image Processing Algorithms and Applications. Wiley, Hoboken (2000)
10. Pomalaza-Racz, C.A., Macgillem, C.D.: An adaptive non linear edge preserving filter. EEE Trans. ASSP **32**(3), 571–576 (1984)
11. Astola, J., Kuosmaneen, P.: Fundamental of Nonlinear Digital Filtering. CRC, Boca Raton (1997)
12. Zhang, S., Karim, M.A.: A new impulse detector for switching median filters. IEEE Signal Process. Lett. **9**(11), 360–363 (2002)
13. Eng, H.-L., Ma, K.-K.: Noise adaptive soft-switching median filter. IEEE Trans. Image Process. **10**(2), 242–251 (2001)
14. Pok, G., Liu, J.-C.: Decision based median filter improved by predictions. In: Proceedings of ICIP, vol. 2, pp. 410–413 (1999)
15. Chan, R.H., Ho, C.-W., Nikolava, M.: Salt and pepper noise removal by median type noise detectors and detail preserving regularization. IEEE Trans. Image Process. **14**(10), 1479–1485 (2005)
16. Srinivasan, K.S., Ebenezer, D.: A new fast and efficient decision-based algorithm for removal of high density impulse noises. IEEE Signal Process. Lett. **14**(4), 189–192 (2007)
17. Jayaraj, V., Ebenezer, D.: A new switching-based median filtering scheme and algorithm for removal of high-density salt and pepper noise in images. EURASIP J. Adv. Signal Process. (2010)
18. Aishwarya, K., Jayaraj, V., Ebenezer, D.: A new and efficient algorithm for the removal of high density salt and pepper noise in images and videos. In: Second International Conference on Computer Modeling and Simulation, pp. 409–413 (2010)
19. Esakkirajan, S., Veerakumar, T., Subramanyam, A.N., PremChand, C.H.: Removal of high density salt and pepper noise through modified decision based unsymmetric trimmed median filter. IEEE Signal Process. Lett. **18**(5), 287–290 (2011)
20. Nair, M.S., Raju, G.: A new fuzzy-based decision algorithm for high-density impulse noise removal. Signal Image Video Process. **6**(4), 579–595 (2012)
21. Saeedi, J., Moradi, M.H., Faez, K.: A new wavelet-based fuzzy single and multi-channel image denoising. Image Vis. Comput. **28**, 1611–1623 (2010)
22. Wang, Z., Bovik, A.C., Sheikh, H.R., Simoncelli, E.P.: Image quality assessement: From error visibility to structural similarity. IEEE Trans. Image Process. **13**(4), 600–612 (2004)
23. Wang, Z., Bovik, A.C.: A universal image quality index. IEEE Signal Process. Lett. **9**(3), 81–84 (2004)
24. Kim, S., Kang, W., Lee, E., Paik, J.: Vaguelette-wavelet decomposition for frequency adaptive image restoration using directional wavelet bases. IEEE Trans. Consumer Electron. **57**(1), 218–2223 (2011)
25. Abdou, I.E., Pratt, W.K.: Quantitative design and evaluation of enhancement/thresholding edge detectors. Proc. IEEE **67**(5), 753–763 (1979)
26. Pratt, W.K.: Digital Image Processing, 2nd edn. Wiley, New York (1991)